

Numerical analysis of attenuation effect of EPS geofoam on stress-waves in civil defense engineering

Zhi-Liang Wang^{a,b,*}, Yong-Chi Li^a, J.G. Wang^c

^aDepartment of Mechanics and Mechanical Engineering, University of Science and Technology of China, Anhui Province, Hefei 230027, PR China

^bCollege of Civil Engineering, Hefei University of Technology, Anhui Province, Hefei 230027, PR China

^cCentre for Protective Technology, National University of Singapore, 10 Kent Ridge Crescent, Singapore 119260, Singapore

Received 20 March 2005; received in revised form 3 April 2006; accepted 11 April 2006

Available online 8 June 2006

Abstract

Civil defense shelters are often constructed below ground to provide protection against blast loading. Concrete has been used extensively as a construction material for the defense layer of the shelters. In order to achieve expected attenuation of blast-induced stress-waves, geofoam or cavity inclusions are sometimes embedded in the concrete layer. This paper studies the attenuation of stress-waves in a concrete medium behind a rectangular inclusion of expanded polystyrene (EPS) geofoam with different dimensions. The effects of EPS geofoam inclusions on the reduction of peak axial stress σ_y and hydrostatic pressure P are studied, respectively. One approximation formula is proposed to correlate the decay factor for peak σ_y to the dimensions of the EPS geofoam inclusion based on numerical simulations. This formula is applicable in defense engineering design to estimate the decay factors at different locations or the dimensions of EPS geofoam when other parameters are prescribed. Finally, the effects of multiple rectangular inclusions of EPS geofoam on stress-waves are numerically investigated.

© 2006 Elsevier Ltd. All rights reserved.

Keywords: Stress-waves; EPS geofoam; Geometric dimension; Decay factor; Empirical formula

1. Introduction

Wave diffraction refers to the propagation direction offset when waves meet certain obstacles such as cavities, crevices and other different media in their transmission courses. At the same time, stress intensities can be greatly reduced, even to zero, behind those obstacles compared with no obstacle cases. This reduction is usually called attenuation or insulation of stress-waves (Achenbach, 1973; Rossmannith and Fournery, 1982). In this paper, the focus is on the reduction of air-blast-induced stress-waves by using EPS geofoam (hereafter called *geofoam*) inclusions in a concrete defense layer.

The attenuation of stress-waves is a current subject of concern in the anti-explosion and shockproof field. With

the development of modern military technology, destructive power and hit rate of new weapons are greatly improved, thus posing a challenge to the protective technology in modern defense engineering. For example, civil defense shelters are widely used to prevent or reduce the damage of underground structures from blasting shock (Yang, 1997). When a civil defense shelter is designed, the attenuation of stress-waves in ground media is a necessary issue to be studied. A new system such as an intelligent defense layer is expected to abate the stress-waves or dissipate their energy.

An intelligent defense layer can be formed through a layered defense structure as shown in Fig. 1 (Li et al., 2004; Wang et al., 2006a, b). This structure consists of three components: a soil cover layer, a protective layer and a support layer. The protective layer has two sub-layers: a projectile shelter layer and a stress distribution layer. The main function of the projectile shelter is to prevent the penetration of projectile. So far, several types of projectile shelter layers have been proposed (Kennedy, 1976; Rohani,

*Corresponding author. Department of Mechanics and Mechanical Engineering, University of Science and Technology of China, Anhui Province, Hefei 230027, PR China. Fax: +86 551 3606459.

E-mail address: zliangw@ustc.edu.cn (Z.-L. Wang).

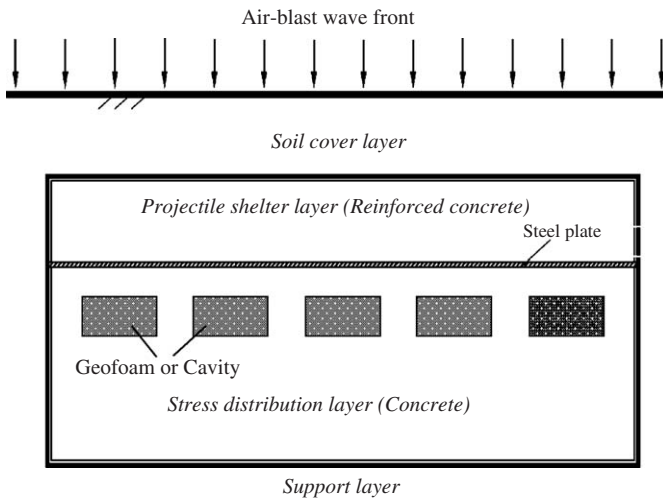


Fig. 1. Schematic drawing for typical defense structure.

1987; Dancygier et al., 1999). The stress distribution layer is usually made up of buffer materials such as foam and other particulates to redistribute blast loading over a larger area and reduce the magnitude of blast-induced stress-waves. However, the understanding for the stress distribution layer is still poor. For example, in practice EPS geofoam block can be embedded into the stress distribution layer to effectively dissipate the energy of stress-waves and thus largely reduce the stress-wave intensity. However, what is the function of EPS geofoam in the attenuation of stress-waves and how to design the EPS geofoam inclusions in defense shelters are still open issues.

Few studies have been performed on the diffraction and attenuation of air-blast-induced stress-waves through geofoam inclusions although the research on anti-explosion theory has been conducted for over 40 yr (Robinson, 1970; Yang, 1997; Mosalam and Mosallam, 2001; Wang and Lu, 2003). EPS geofoam is a lightweight polymeric material which is made by expansion of raw plastic beads. When expanded, the EPS beads become spherical-shaped particles, and each contains closed hollow cells. Therefore, EPS beads are air-filled spherical particles. So far, EPS geofoam has been widely used in geotechnical engineering because of its excellent mechanical properties such as lightweight fill, reduction of pressure, noise and vibration damping, thermal insulation and compressible inclusions (Aytekin, 1997; Zou and Leo, 1998; Horvath, 1997, 2004). It is also expected that EPS geofoam can better absorb energy from blasting and seismic shocks and reduce the magnitude of stress-waves through using EPS geofoam inclusions in a defense layer. The technique on using compressible inclusions in stabilizing structures for earthquake loading has been experimentally established (Riad and Horvath, 2004). This technique is easily implemented in a short time span, and does not produce harmful effects on nearby structures (Hazarika et al., 2003; Hazarika and Okuzono, 2004). In civil defense engineering, EPS geofoam as compressible inclusions may be placed into the stress

distribution layer to absorb the blast-induced stress-waves through its damping and diffusing functions.

In this paper, numerical analyses are carried out to study the effect of embedded EPS geofoam inclusions on the attenuation of stress-waves in a concrete medium. Firstly, the effects of a single rectangular EPS inclusion on the attenuation of peak axial stress σ_y and hydrostatic pressure P are numerically investigated. Furthermore, a detailed inspection on the effect of geofoam density on stress-waves is made. Secondly, based on these numerical results, an empirical formula is then proposed to correlate the decay factor of axial stress σ_y to EPS geofoam dimensions. Finally, the screen effects of multiple rectangular EPS inclusions on the attenuation of stress-waves are analyzed, and the results are compared with those of a single rectangular EPS inclusion case. This paper seeks to provide helpful means for the design of intelligent defense layer in practice.

2. Numerical tool, computational model and constitutive laws of materials

2.1. Numerical tool

The commercial software, LS-DYNA from the *Livermore Software Technology Corporation*, is employed in this paper to carry out all computations. LS-DYNA is a general-purpose finite element code for analyzing the large deformation dynamic response of structures. It can handle either two- or three-dimensional problems for high-speed impact and explosion with an explicit time integration scheme which is a slight modification of the standard central difference method (LSTC, 2003).

2.2. Computational model

A typical two-dimensional computational model is shown in Fig. 2. In this model, the stress distribution layer is composed of concrete medium and embedded with a rectangular EPS inclusion. The problem domain is taken as $600.0\text{ cm} \times 300.0\text{ cm}$ and the EPS inclusion is $2l$ in length and h in width. The distance between the x -axis and the top of EPS geofoam is denoted as e . Other dimensions are shown in Fig. 2. Therefore, the dimension Y is

$$Y = y + e + h, \quad (1)$$

where y is the relative distance between point A and the lower side of the cavity.

Only right-half domain illustrated in Fig. 2b is computed because of symmetry. Hence, its boundary conditions are specified as follows: the top is traction boundary, right and lower sides are non-transmission boundaries (free reflection), and the left side is symmetric boundary. Air-blast induced load is approximated by a triangular pulse load shown in Fig. 3 (Guruprasad and Mukherjee, 2000) and evenly applied to the top of the computational domain. In the present study, the peak value Q_{\max} is taken as 120 MPa

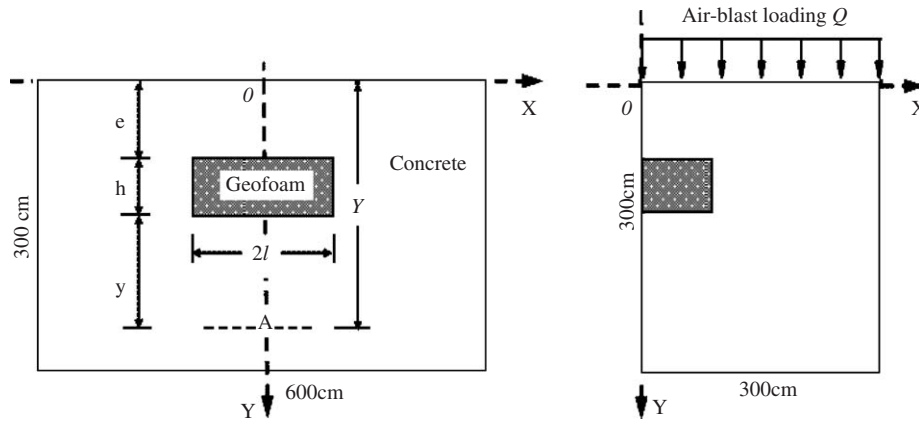


Fig. 2. Computational domain and dimensions for scheme of rectangular geofoam inclusion: (a) whole domain and (b) half domain for computation.

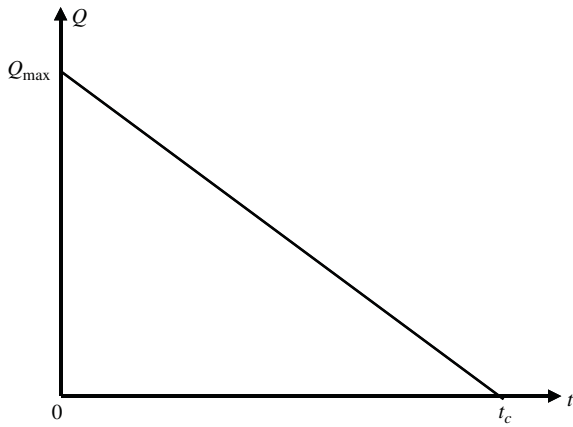


Fig. 3. Triangular impulse loading for explosion.

and occurs at time $t_{\max} = 0.0 \mu\text{s}$ (microsecond). This overpressure then decreases linearly to zero at time $t_c = 100.0 \mu\text{s}$. Such an overpressure corresponds to the charge weight of 885 kg and stand-off distance of 5 m in the air (Wang et al., 2006b).

2.3. Constitutive laws for materials

2.3.1. Constitutive model for concrete

LS-DYNA currently contains about 200 constitutive models which are suitable for a wide range of material behaviors. This paper adopts the material model 3 called “MAT PLASTIC KINEMATIC” in LS-DYNA (Hallquist, 1998) to model the material behavior of concrete under dynamic load. This model considers both isotropic and kinematic hardening plasticity as well as strain rate effects. The yield stress of the material is computed based upon the relation

$$\sigma_y = \left[1 + \left(\frac{\dot{\epsilon}}{C} \right)^{1/\eta} \right] (\sigma_0 + \beta E_p \epsilon_{\text{eff}}^p), \quad (2)$$

where C , η and $0 < \beta < 1$ are user-defined input constants, E_p is plastic hardening modulus, ϵ_{eff}^p is equivalent plastic strain, σ_0 is initial yield strength and the strain rate $\dot{\epsilon}$ is given by as follows:

$$\dot{\epsilon} = \sqrt{\dot{\epsilon}_{ij} \dot{\epsilon}_{ij}}. \quad (3)$$

The combination of isotropic and kinematic hardening is obtained by varying the value of β between 0 and 1. For β equal to 0 and 1, respectively, kinematic and isotropic hardening is obtained.

Main material properties such as the mass density, the Young's modulus, the Poisson's ratio, the yield stress and the tangent modulus are taken to be 2240 kg/m^3 , 30 GPa, 0.18, 30 MPa and 2.2 GPa, respectively.

2.3.2. Constitutive model for crushable foam

The plasticity constitutive model for crushable foams (Krieg, 1972) is employed to describe the mechanical properties of EPS geofoam. This constitutive model was successfully applied to EPS geofoam (Zhang et al., 1998) and implemented into the LS-DYNA to simulate the dynamic behavior of crushable foams through volumetric deformations (Hallquist, 1998; LSTC, 2003).

A typical curve of hydrostatic pressure versus volumetric strain is illustrated in Fig. 4. This curve is required to be input into LS-DYNA with tabulated data. The deviatoric deformation is described by a plasticity potential theory. Its plastic yield function, ϕ , is a pressure-dependent function as

$$\phi = J_2 - [a_0 + a_1 P + a_2 P^2], \quad (4)$$

where a_0 , a_1 , and a_2 are material constants, P is the hydrostatic pressure, J_2 is the second invariant of deviatoric stress which is

$$J_2 = \frac{1}{2} s_{ij} s_{ij}. \quad (5)$$

The implementation of this model is straightforward if associated flow rule is used. The maximum volumetric strain in compression is used as loading factor and stored

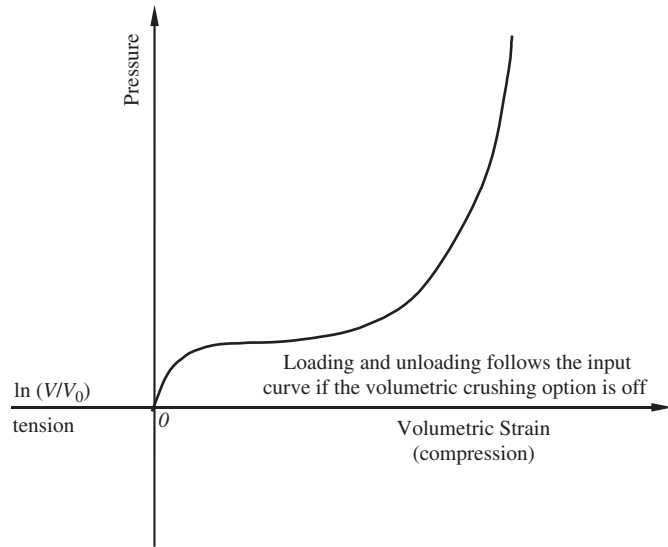


Fig. 4. Pressure versus volumetric strain curve for crushable foam model.

in each incremental step. When new compressive volumetric strain exceeds the stored value, the deformation is in loading. For an incremental step, updated trial stress, s_{ij}^* , is scaled back by using a simple radial return algorithm (Hallquist, 1998):

$$s_{ij}^{n+1} = \left(\frac{a_0 + a_1 P + a_2 P^2}{J_2} \right)^{1/2} s_{ij}^* \quad (6)$$

Because the yielding surface has no strain hardening, there exists

$$J_2 = \frac{1}{3} \sigma_y^2 \quad (7)$$

in which σ_y is the uniaxial yield stress. From Eqs. (4) and (7), the yield stress is obtained as

$$\sigma_y = \sqrt{3(a_0 + a_1 P + a_2 P^2)}. \quad (8)$$

As a summary, this model has following parameters: ρ_0 (initial density), K (bulk modulus), G (shear modulus) and p_c (pressure cutoff for tensile fracture). If hydrostatic tension exceeds the cutoff value, the pressure is set to the cutoff value and deviatoric stress tensor keeps zero.

As aforementioned, the volumetric strain versus hydrostatic pressure is given in tabulated data and is input with increase of compression. This volumetric strain is expressed in terms of natural logarithm of relative volume, V/V_0 , where V is the current volume and V_0 is the initial volume. The volumetric strain is negative when in compression. For EPS blocks with three densities of 12, 21 and 27 kg/m³ (Zou and Leo, 1998), the model parameters are listed in Table 1. Their volumetric strain versus hydrostatic pressure curves are given in Table 2.

Table 1
Main parameters of EPS geofoam

ρ_0 (kg/m ³)	G (MPa)	K (MPa)	a_0 (kPa ²)	a_1 (kPa)	a_2	P_c (kPa)
27.0	2.92	1.62	5535.36	8.928	0.0036	−42.0
21.0	2.12	1.13	2246.80	10.428	0.0121	−27.0
12.0	1.22	0.61	529.0	3.220	0.005	−12.0

3. Numerical investigations

3.1. Single EPS geofoam inclusion

This section will numerically investigate the effect of geofoam inclusions on the reduction of stress-waves if the EPS density is 27 kg/m³. A dimensionless variable, ‘decay factor’ or DF , is defined as follows to measure the attenuation of stress-waves:

$$DF = \frac{\sigma_0 - \sigma}{\sigma_0}, \quad (9)$$

where σ_0 denotes the peak value of a stress component such as σ_x , σ_y and P at a specified position when no inclusions is present. σ denotes the peak value of the same stress component at the same position when EPS geofoam inclusion exists. Larger DF means better attenuation effect of geofoam inclusions on stress-waves.

3.1.1. Effect of geofoam length l

Five lengths of EPS geofoam are considered in this computation: 0.0, 0.3, 0.6, 0.9 and 1.2 m. Other geometrical parameters are taken as $e = 0.9$ m and $h = 0.3$ m. The numerical results are illustrated in Figs. 5–7. Fig. 5 shows the relationship of decay factors for peak σ_y and hydrostatic pressure P and relative distance y . It reveals that the geofoam length has significant effect on the attenuation of peak σ_y and P , and their attenuation patterns are quite different. For instance, at point B ($x = 0.0$ m, $Y = 1.4$ m, $y = 0.2$ m), the DF almost reaches 1.0 for the σ_y but only 0.90 for the P when $l = 1.2$ m. However, at point C ($X = 0.0$ m, $Y = 2.2$ m, $y = 1.0$ m), the decay factor is 0.44 for σ_y and 0.29 for P when $l = 0.3$ m. Furthermore, the DF becomes smaller when relative distance y increases (for the same l). Fig. 6 shows the hydrostatic pressure P versus time t at point D ($X = 0.0$ m, $Y = 1.65$ m, $y = 0.45$ m) which is below the geofoam inclusion. With increase of geofoam length l , the peak value of P gradually decreases, and the arrival time of peak value gradually lags. The relationship of peak σ_y versus time at point E ($X = 0.0$ m, $Y = 2.3$ m, $y = 0.5$ m) is presented in Fig. 7. It is obvious that the peak σ_y decreases with increase of the geofoam length l . For example, the peak value when $l = 0.9$ m is approximately quarter of the peak value when $l = 0.3$ m.

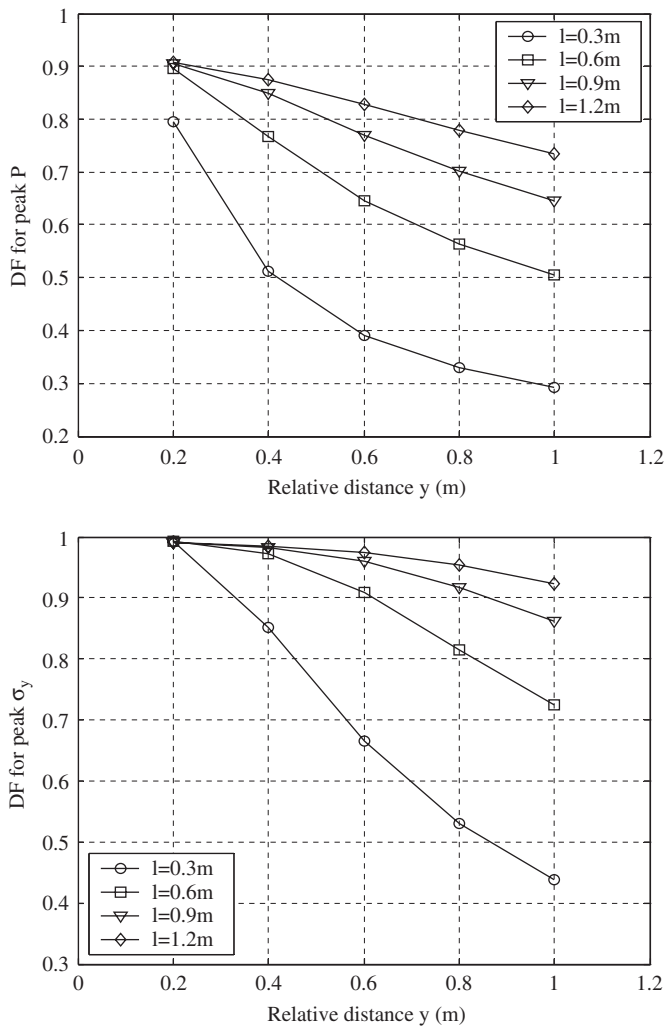
Table 2

Tabulated data of hydrostatic compressive stress–strain for EPS geofoam

Hydrostatic pressure (kPa)				Strain			
Item	$\rho_0 = 27 \text{ (kg/m}^3\text{)}$	$\rho_0 = 21 \text{ (kg/m}^3\text{)}$	$\rho_0 = 12 \text{ (kg/m}^3\text{)}$	Item	$\rho_0 = 27 \text{ (kg/m}^3\text{)}$	$\rho_0 = 21 \text{ (kg/m}^3\text{)}$	$\rho_0 = 12 \text{ (kg/m}^3\text{)}$
p_1	0.000	0.000	0.000	ε_1	0.0000	0.0000	0.0000
p_2	4.918	10.000	9.689	ε_2	−0.0053	−0.0123	−0.0201
p_3	10.109	14.286	14.879	ε_3	−0.0113	−0.0165	−0.0319
p_4	24.863	39.895	20.069	ε_4	−0.0207	−0.0328	−0.0458
p_5	42.721	51.286	24.567	ε_5	−0.0340	−0.0488	−0.0632
p_6	68.306	61.429	29.066	ε_6	−0.0475	−0.0645	−0.0820
p_7	84.973	65.714	34.602	ε_7	−0.0648	−0.0800	−0.1110
p_8	95.082	70.000	39.792	ε_8	−0.0859	−0.0953	−0.1332
p_9	101.634	74.286	47.405	ε_9	−0.1090	−0.1178	−0.1706
p_{10}	104.645	81.429	49.481	ε_{10}	−0.1296	−0.1398	−0.1815

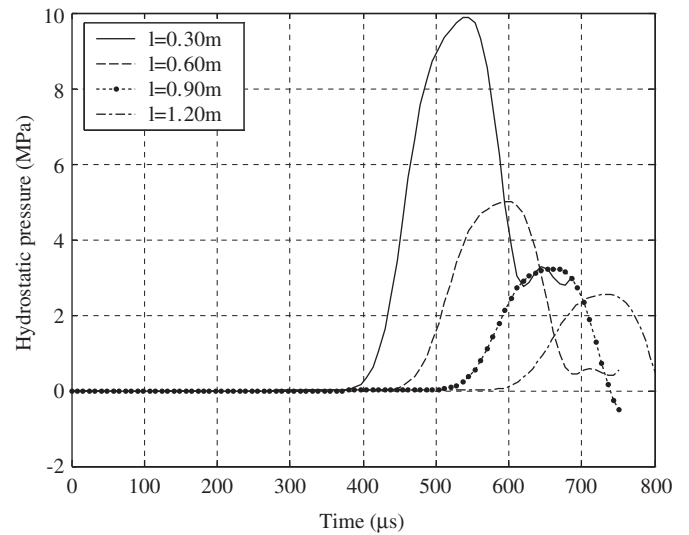
(i) Pressure is positive when in compression.

(ii) Strain is the natural logarithm of the relative volume and is negative in compression.

Fig. 5. Variations of the decay factors with different lengths l of geofoam inclusion: (a) hydrostatic pressure P and (b) axial stress σ_y .

3.1.2. Effect of geofoam width h

The effect of geofoam width on the attenuation of stress-wave is investigated in this section. The width h of geofoam

Fig. 6. Effect of length of geofoam inclusion on hydrostatic pressure history at point D .

inclusion is taken as 0.3, 0.6, 0.9, 1.2 and $l = e = 0.3 \text{ m}$. Numerical results are depicted in Figs. 8 and 9. Fig. 8 shows that the width h of EPS geofoam has little influence on decay factors for both σ_y and P . The decay factor is larger for σ_y than for P . For example, the DF is almost 1.0 for the peak σ_y but only 0.80 for the peak P at point F ($X = 0.0 \text{ m}$, $Y = 1.7 \text{ m}$, $y = 0.2 \text{ m}$) when $h = 1.2 \text{ m}$. Fig. 9 compares the hydrostatic pressure P versus time curves at the point ($X = 0.0 \text{ m}$, $y = 0.50 \text{ m}$) for different widths h . The peak values are almost identical except some time lag when the h is 0.15, 0.3, 0.6, 0.9 and 1.2 m, respectively.

3.1.3. Effect of geofoam position e

The effect of geofoam position is studied here. The position e varies as 0.3, 0.6, 0.9 and 1.2 m. Other dimensions are taken as $l = 0.3 \text{ m}$ and $h = 0.3 \text{ m}$. The effect of geofoam position on the decay factor is shown in Fig. 10a for the peak σ_y and Fig. 10b for hydrostatic

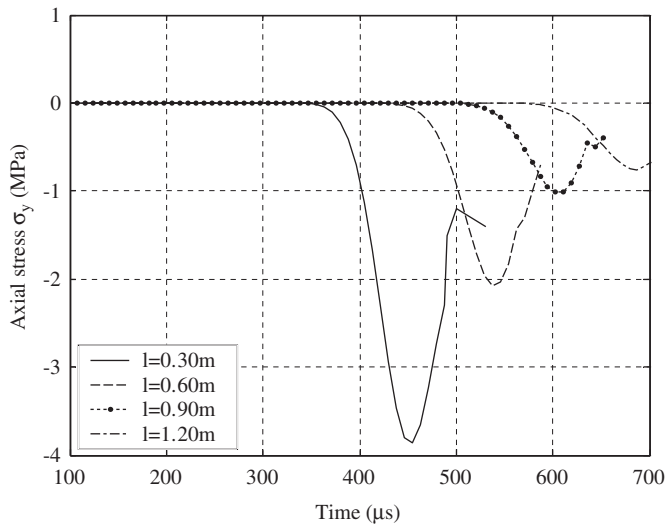


Fig. 7. Effect of length of geofoam inclusion on axial stress history at point E.

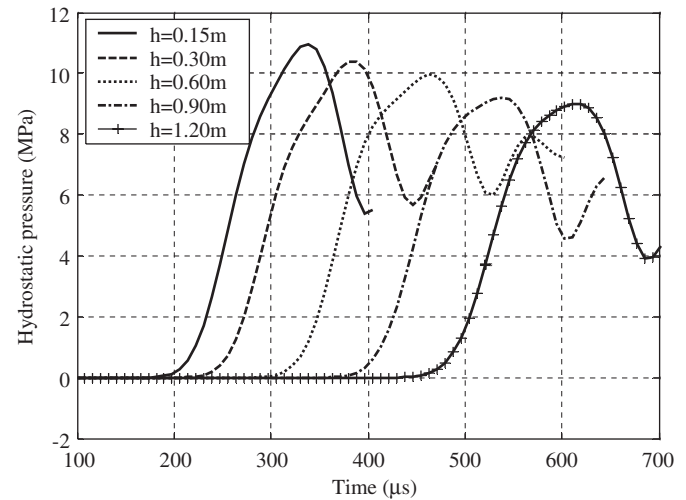


Fig. 9. Effect of width of geofoam inclusion on hydrostatic pressure history at $y = 0.50$ m point on Y-axis.

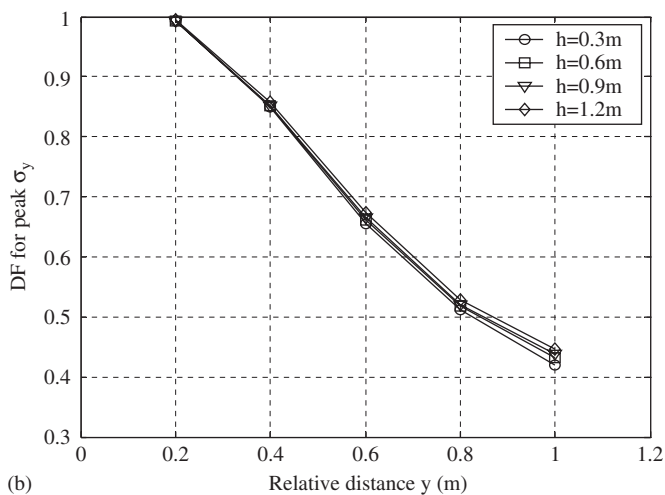
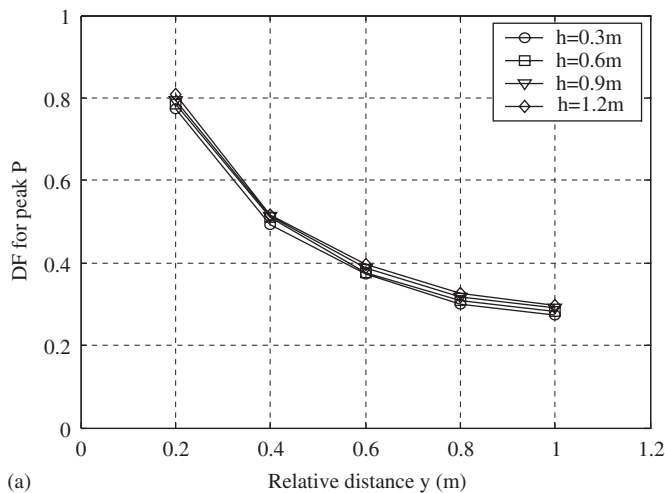


Fig. 8. Variations of the decay factors with different widths h of geofoam inclusion: (a) hydrostatic pressure P and (b) axial stress σ_y .

pressure P . In general, the decay factor is larger for the peak σ_y than for the peak P . It may be easily noticed that the effect of position e on decay factors is negligible. This phenomenon can be also observed from the time-hydrostatic pressure curves at $y = 0.5$ m point shown in Fig. 11. The peak values have almost the same magnitude but arrival time is lagged with increase of position e .

3.1.4. Effect of geofoam density ρ

EPS geofoam exhibits not only highly nonlinear mechanical behavior but also density dependent characteristic (Hazarika and Okuzono, 2004; Chun et al., 2004; Hazarika, 2006). Above numerical simulations were carried out for the geofoam inclusions with the density of 27 kg/m^3 . This section will investigate the density effect of EPS inclusions on attenuation of stress-waves. In order to be representative, the adopted density ranges from 12 to 21 kg/m^3 .

The effect of geofoam density on the reduction of the peak σ_y is shown in Fig. 12. This figure shows that the geofoam density has little influence on the peak σ_y in this simulation. It is noted that this result is obtained for the big difference of mechanical characteristics of EPS geofoam and concrete. This may be that the geofoam block is too soft to affect the decay factor in the concrete medium. However, EPS geofoam can perfectly absorb the energy of stress-wave from the surrounding concrete.

3.1.5. Empirical formula for decay factor

Based on the above numerical results, the effects of ρ , h and e on axial stress σ_y are negligible. Therefore, the DF for peak σ_y is a function of two variables l and y :

$$DF = f(l, y). \quad (10)$$

According to the computational points shown in Fig. 5b, we further choose one h (0.3 m), four l (0.3, 0.6, 0.9 and 1.2 m) and five y (0.2, 0.4, 0.6, 0.8 and 1.0 m) for

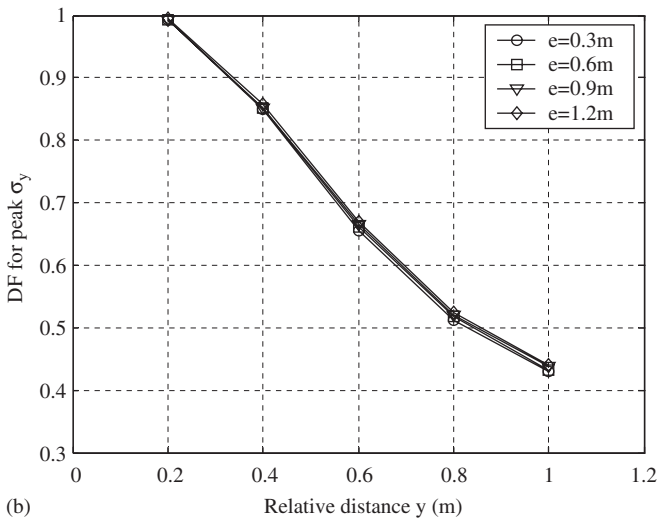
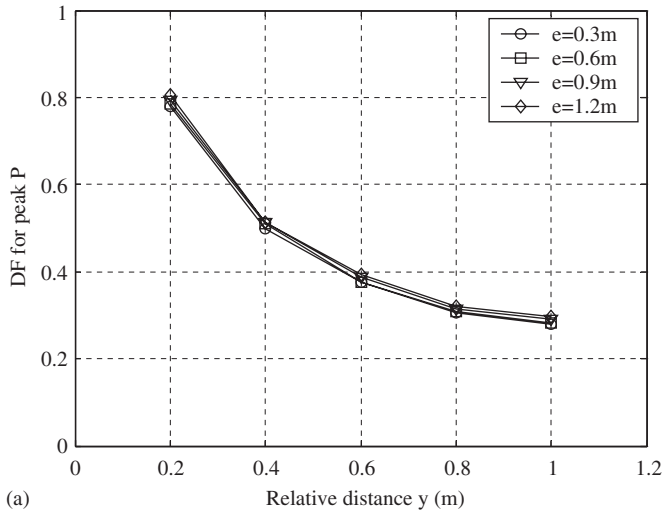


Fig. 10. Variations of the decay factors with different positions e of geofoam inclusion: (a) hydrostatic pressure P and (b) axial stress σ_y .

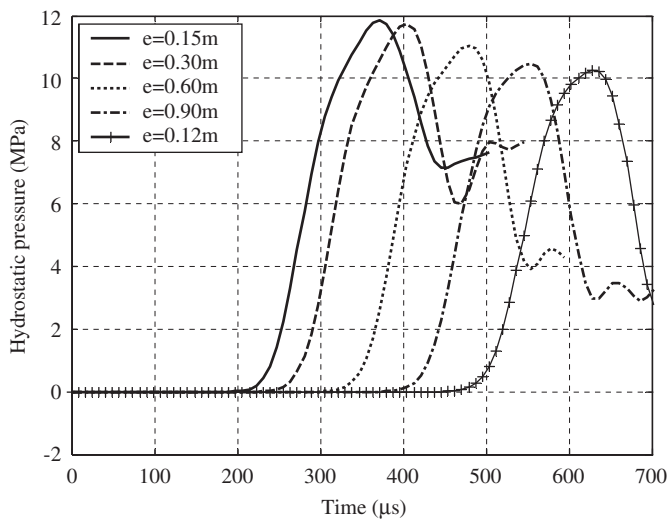


Fig. 11. Effect of position of geofoam inclusion on hydrostatic pressure history at $y = 0.50$ m point on Y -axis.

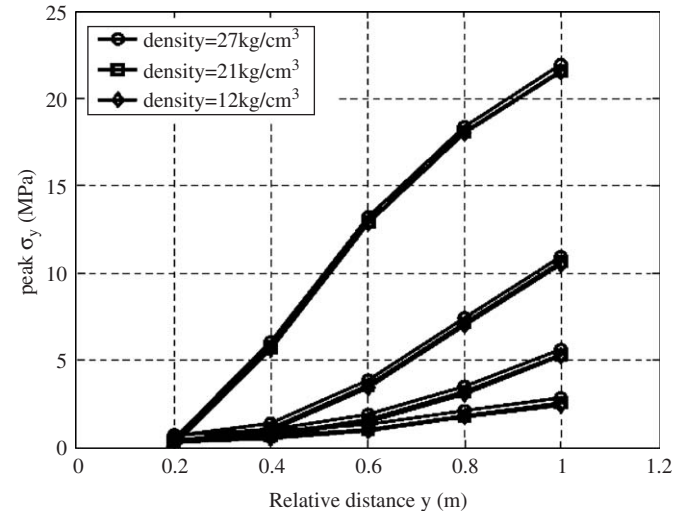


Fig. 12. Effect of geofoam initial density on reduction of peak axial stress.

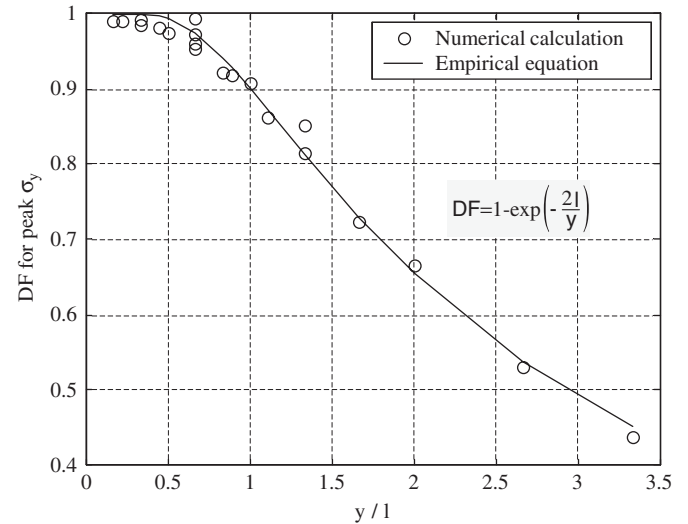


Fig. 13. Comparison between empirical formulae and numerical results of the decay factors for peak σ_y .

computation. Following regression curve for the decay factor of the peak σ_y is obtained:

$$DF = 1 - \exp\left(-\frac{2l}{y}\right). \quad (11)$$

Fig. 13 compares the numerical results and empirical formula of Eq. (11). Good agreements can be found. This empirical formula shows that DF increases when the l increases or the y decreases. The DF is equal to unity when y/l is zero.

Obviously, Eq. (11) can estimate the length l (or the whole length $2l$) of geofoam block if the expected DF at the relative distance y is given. When DF and length l are pre-determined, Eq. (11) can also estimate the nearest safe position (i.e. y_{\min}). In civil defense shelter design, some criterion sets the DF value at specified location behind the

geofoam inclusion to ensure the safety of underground structures. For this design purpose, Eq. (11) can be used to estimate the minimum length (l_{\min}) of EPS geofoam inclusion. As an example, l_{\min} is not less than 0.347 m when $y = 1.0$ m and $DF \geq 0.5$.

3.2. Multiple EPS geofoam inclusions

The above results on single EPS inclusion indicate that the EPS geofoam can have great influence on the attenuation of stress-waves. In practice, single inclusion cannot form a screen against stress-waves especially in lateral direction. This screen may be formed by using multiple inclusions of EPS geofoam as shown in Fig. 14. A total of five rectangular geofoam inclusions (90.0 cm \times 30.0 cm) are embedded in this concrete medium. The spacing between two neighborhood geofoam inclusions is 25.0 cm. Fig. 15 shows the finite element model for computations. It consists of 7200 quadrilateral elements and 7382 nodes. The same loading in Fig. 3 is applied to the top. In addition, the computation parameters for single inclusion case are used for both concrete and EPS geofoam (density = 27 kg/m³).

The screen effects of single and multiple geofoam inclusions on decay factors of peak σ_y and P are compared

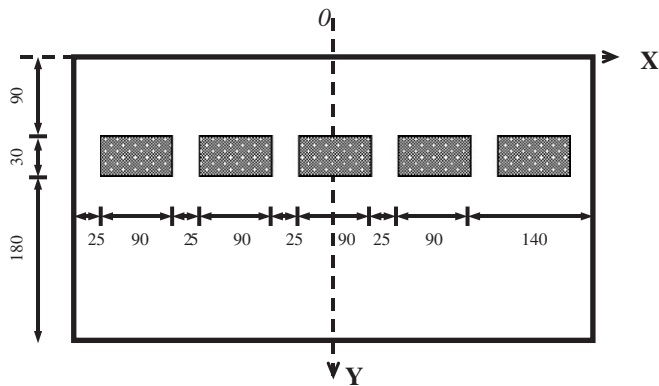


Fig. 14. Computational domain and dimensions for scheme of multiple rectangular geofoam inclusions (unit: cm).

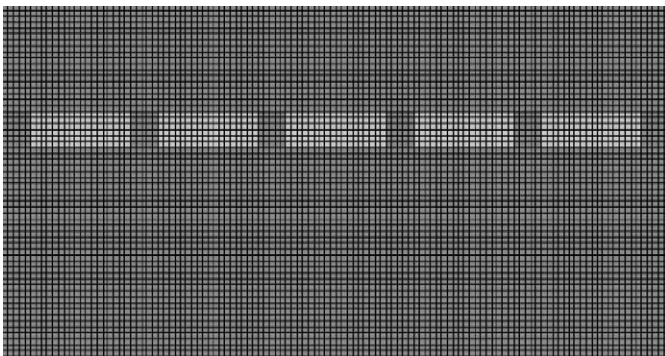


Fig. 15. Finite element grid for multiple geofoam inclusions.

in Fig. 16 when $e = 0.9$ m and $h = 0.3$ m. Fig. 16a clearly shows that decay factor for the peak σ_y is much higher for multiple geofoam inclusions than for single geofoam inclusion. The effect of multiple geofoam inclusions ($l = 0.45$ m) is rather close to that of the single geofoam inclusion with $l = 0.60$ m when the relative distance is shorter than 1.0 m. Fig. 16b compares the decay factors of the peak P in the lateral direction at seven sample points ($y = 1.0$ m) between multiple geofoam inclusions and single geofoam inclusion. With increase of lateral distance X , decay factors for the case of multiple geofoam inclusions fluctuate around 0.65 and a screen against stress waves is formed. Obviously, the attenuation of multiple geofoam inclusions is much better than that of single geofoam inclusion because decay factor for single geofoam case, whether $l = 0.45$ or 0.60 m, reduces to zero when the lateral distance is larger than 1.5 m.

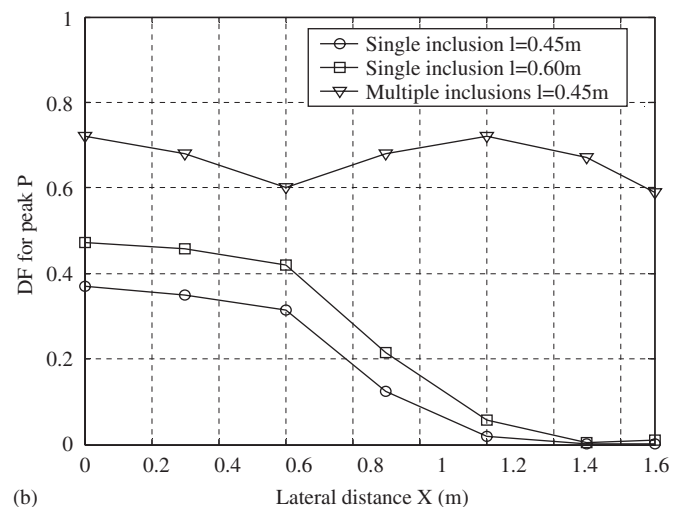
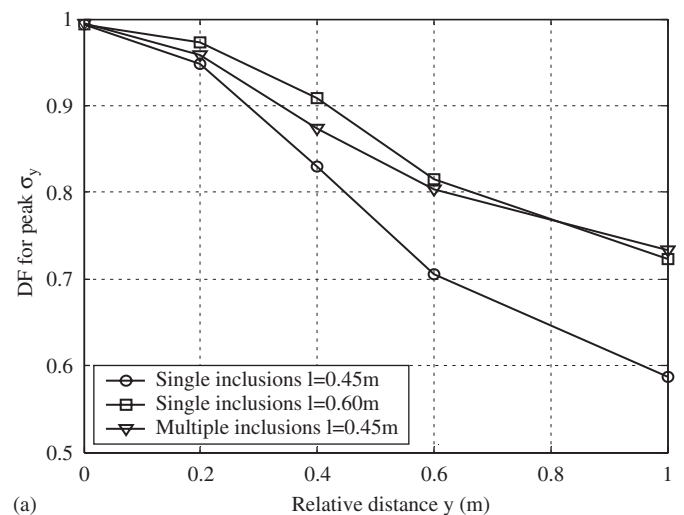


Fig. 16. Comparisons of screen effect between single and multiple rectangular inclusions of EPS geofoam: (a) axial stress σ_y and (b) hydrostatic pressure P .

4. Conclusions

The diffraction and attenuation of stress-waves in a concrete medium with embedded rectangular inclusions of EPS blocks are studied numerically. An empirical formula is proposed for the attenuation of the peak axial stress based on the numerical results. In addition, the effects of multiple rectangular inclusions of geofoam are investigated. From this study, the following conclusions may be drawn.

First, the existence of EPS geofoam inclusions has important effects on the attenuation of stress-waves in a concrete defense layer. For a rectangular geofoam inclusion, the decay factor largely depends on the length l of the inclusion while the width h has little effect. The decay factor is generally larger for the peak axial stress σ_y than for the peak hydrostatic pressure P .

Second, an empirical formula is proposed to correlate decay factor to the length of geofoam inclusion and the location to be protected. This formula can be used to estimate the minimum length of geofoam inclusion, or minimum safe distance y_{\min} when the decay factor is given. This provides a helpful tool to design an intelligent defense layer in civil defense engineering.

Third, multiple rectangular inclusions of EPS geofoam can preferably form a screen against stress-waves in practice. The decay factors are much higher for multiple EPS inclusions than for a single geofoam inclusion when the dimensions of each inclusion and its position are the same. Multiple EPS geofoam inclusions are even good at forming a screen against stress-waves in the lateral direction.

Acknowledgment

This work was partially supported by the Post-doctoral Science Foundation of China (Project no. 2004036468).

References

- Achenbach, J.D., 1973. *Wave Propagation in Elastic Solids*. North-Holland, Amsterdam (pp. 1–69).
- Aytakin, M., 1997. Numerical modeling of EPS geofoam used with swelling soil. *Geotextiles and Geomembranes* 15 (1–3), 133–146.
- Chun, B.-S., Lim, H.-S., Sagong, M., Kim, K., 2004. Development of a hyperbolic constitutive model for expanded polystyrene (EPS) geofoam under triaxial compression tests. *Geotextiles and Geomembranes* 22 (4), 223–237.
- Dancygier, A.N., Yankelevsky, D.Z., Baum, H., 1999. Behavior of reinforced concrete walls with internal plaster coating under exterior hard projectile impact. *ACI Materials Journal* 91 (1), 116–125.
- Guruprasad, S., Mukherjee, A., 2000. Layered sacrificial claddings under blast loading. Part I—analytical studies. *International Journal of Impact Engineering* 24, 957–973.
- Hallquist, J.O., 1998. *LS-DYNA Theoretical Manual*, California, USA.
- Hazarika, H., 2006. Stress–strain modeling of EPS geofoam for large-strain applications. *Geotextiles and Geomembranes* 24 (2), 79–90.
- Hazarika, H., Okuzono, S., 2004. Modeling the behavior of a hybrid interactive system involving soil, structure and EPS geofoam. *Soils and Foundations* 44 (5), 149–162.
- Hazarika, H., Okuzono, S., Matsuo, Y., 2003. *Seismic Stability Enhancement of Rigid Non-Yielding Structures*, 2. International Society of Offshore and Polar Engineers (ISOPE) Transactions, Honolulu, USA, pp. 697–702.
- Horvath, J.S., 1997. The compressive inclusion function of EPS geofoam. *Geotextiles and Geomembranes* 15, 77–120.
- Horvath, J.S., 2004. Cellular geosynthetics in transportation applications. *Geotechnical Special Publication* 1261, 627–636.
- Krieg, R.D., 1972. *A Simple Constitutive Description for Soils and Crushable Foam*. SCDR-72-0883. Sandia National Laboratories, Albuquerque, NM.
- Kennedy, R.P., 1976. Review of procedures for the analysis and design of concrete structure to resist missile impact effects. *Nuclear Engineering and Design* 37 (2), 183–203.
- Li, Y.C., Wang, X.J., Hu, X.Z., 2004. Study on layered design and its defending function. Technical Report of National Defense Engineering, USTC, China, 55pp.
- Livermore Software Technology Corporation (LSTC), 2003. *LS-DYNA Keyword User's Manual*, California, USA.
- Mosalam, K.M., Mosallam, S.A., 2001. Nonlinear transient analysis of reinforced concrete slabs subjected to blast loading and retrofitted with CFRP composites. *Composites Part B: Engineering* 32 (8), 623–636.
- Riad, H.L., Horvath, J.S., 2004. Analysis and design of EPS–geofoam embankments for seismic loading. *Geotechnical Special Publication* 126 (II), 2028–2037.
- Robinson, D.N., 1970. A displacement bound principle for elastic-plastic structures subjected to blast loading. *Journal of the Mechanics and Physics of Solids* 18 (1), 65–80.
- Rohani, B., 1987. Shielding methodology for conventional kinetic energy weapons. Technical Report SL-8f-8. U.S. Army engineering, Waterways Experimental Station, Vicksburg M. S, pp. 23–46.
- Rossmannith, H.P., Fourney, W.L., 1982. Fracture initiation and stress wave diffraction at cracked interfaces in layered media: 1. Brittle–brittle-transition. *Rock Mechanics* 14, 209–233.
- Wang, Z., Lu, Y., 2003. Numerical analysis on dynamic deformation mechanism of soils under blast loading. *Soil Dynamics and Earthquake Engineering* 23, 705–724.
- Wang, Z.L., Li, Y.C., Wang, J.G., 2006a. Study of stress waves in geomedia and effect of a soil cover layer on wave attenuation using a 1-D finite-difference method. *Computers & Geosciences* 32(9), in press.
- Wang, Z.L., Wang, J.G., Li, Y.C., Leung, C.F., 2006b. Attenuation effect of artificial cavity on air-blast waves in an intelligent defense layer. *Computers and Geotechnics* 33 (2), 132–141.
- Yang, Z., 1997. Finite element simulation of response of buried shelters to blast loadings. *Finite Elements in Analysis and Design* 24, 113–132.
- Zhang, J., Kikuchi, N., Li, V., Yee, A., Nusholtz, G., 1998. Constitutive modeling of polymeric foam material subjected to dynamic crash loading. *International Journal of Impact Engineering* 21 (5), 369–386.
- Zou, Y., Leo, C.H., 1998. Laboratory studies on engineering properties of expanded polystyrene (EPS) material for geotechnical applications. In: *Second International conference on Ground Improvement Techniques*, Singapore. pp. 581–588.